Electronic Supplementary Material (ESI) for Journal of Materials Chemistry A.

Supplementary Information

Ultra-highly active Ir-Ru-B/CeO_2 catalyst for hydrogen generation from hydrazine monohydrate

Yu-Ping Qiu[a], Wei-Zhen Wang[b], Mu-Hua Chen[a], Qing Shi[a], Zhi-Qing Yang[b], Ping Wang[a]*

[a]School of Materials Science and Engineering, South China University of Technology, Guangzhou 510641, P.R. China

[b]Shenyang National Laboratory for Materials Science, Institute of Metal Research, Chinese Academy of Sciences, Shenyang 110016, P.R. China

*Corresponding author. Tel: +86 20 3938 0583; e-mail: mspwang@scut.edu.cn (P. Wang)

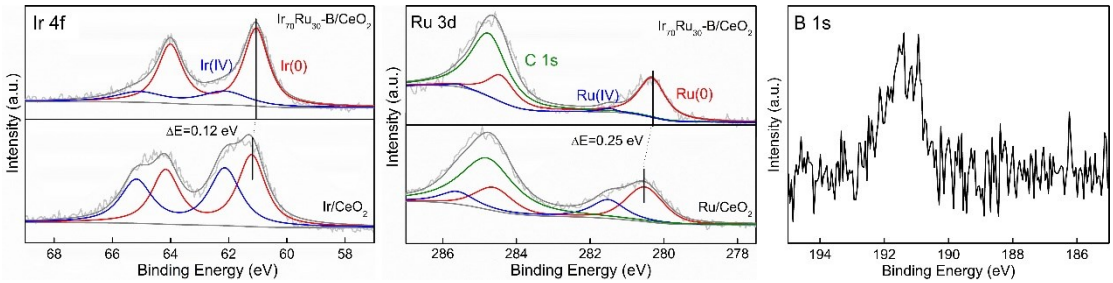

Figure S1. A comparison of XPS spectra of the $Ir_{70}Ru_{30}$-B/CeO_2 catalyst and the relevant Ir/CeO_2 and Ru/CeO_2 reference samples in the Ir 4f, Ru 3d and B 1s regions.

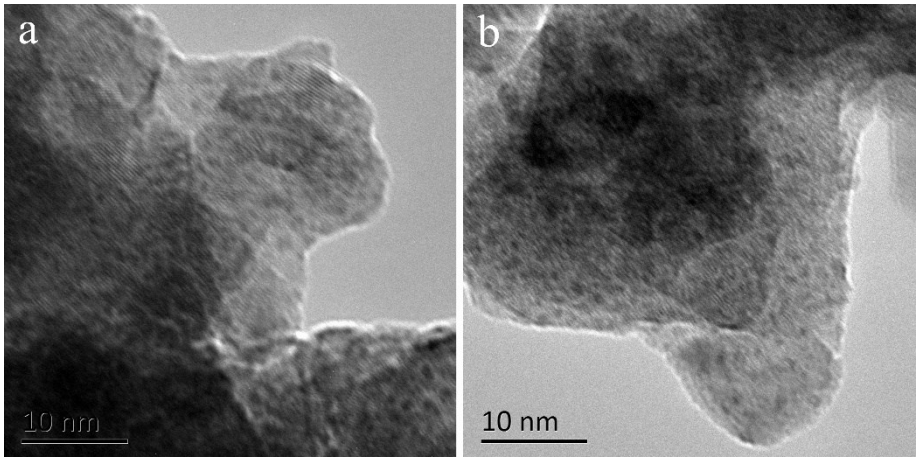

Figure S2. Representative TEM images of the $Ir_{70}Ru_{30}$-B/CeO_2 sample at different states: (a) as-prepared; (b) post-annealed at 600 °C.

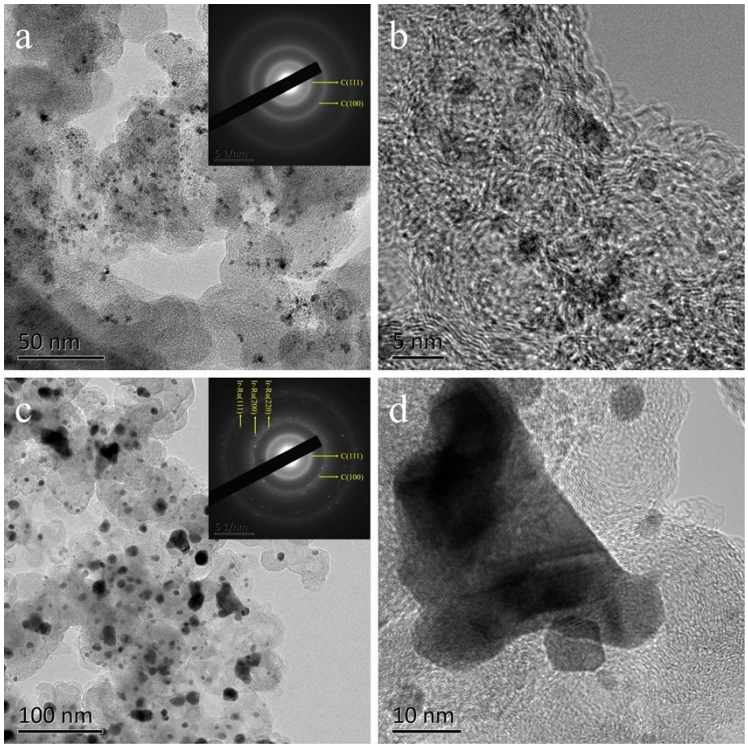

Figure S3. Representative TEM images of the $Ir_{70}Ru_{30}$-B/C sample at different states: (a, b) as-prepared; (c, d) post-annealed at 600 °C. The insets in (a) and (c) show the corresponding SAED patterns, respectively. The loading amount of metal was 30.0 wt% with a comparable loading density to that of $Ir_{70}Ru_{30}$-B/CeO_2 sample.

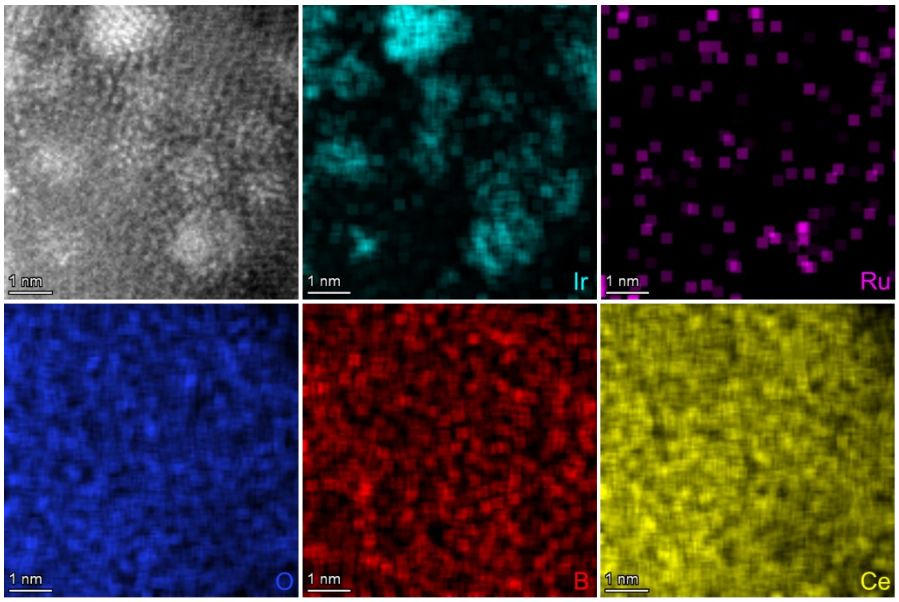

Figure S4. Atomic resolution HAADF-STEM image and corresponding EDS elemental mapping results of the as-prepared $Ir_{70}Ru_{30}$-B/CeO_2 catalyst.

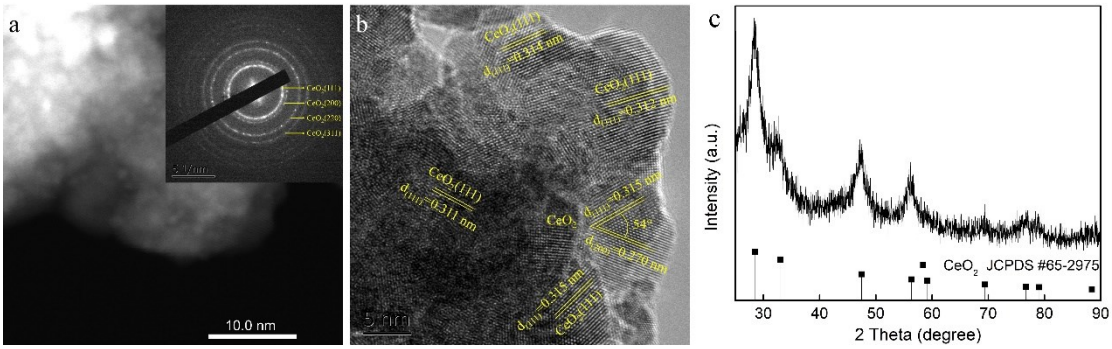

Figure S5. (a) HAADF-STEM image, (b) HRTEM image and (c) XRD pattern of the post-used $Ir_{70}Ru_{30}$-B/CeO_2 catalyst after ten cyclic usage. The inset in (a) shows the SAED pattern.

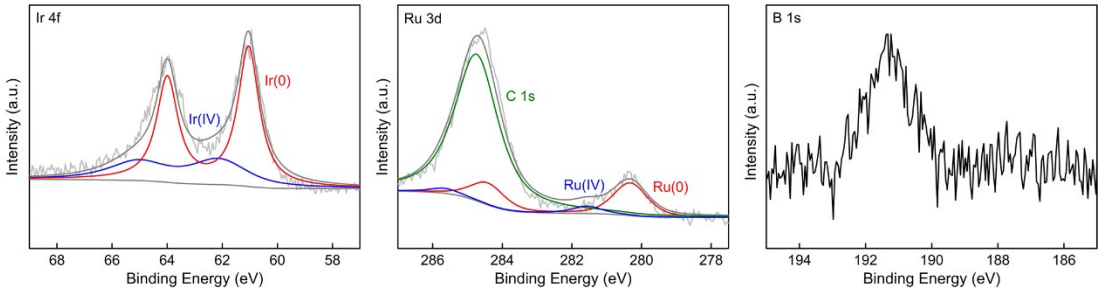

Figure S6. XPS spectra of post-used $Ir_{70}Ru_{30}$-B/CeO_2 catalyst after ten cyclic usage in the Ir 4f, Ru 3d and B 1s regions.

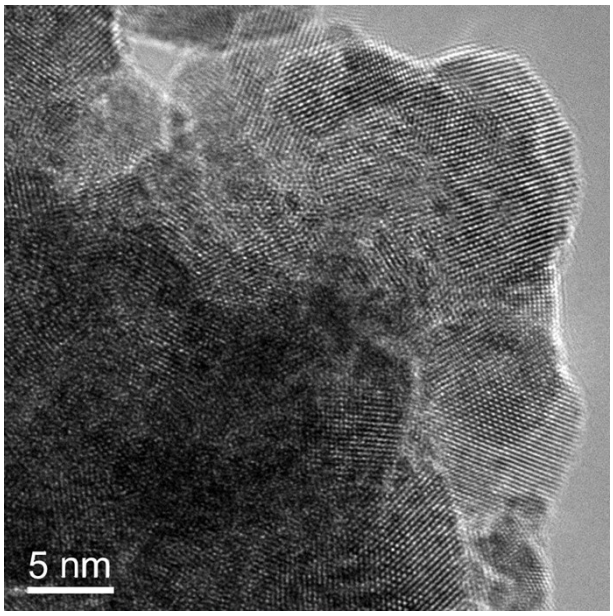

Figure S7. A representative TEM image of the $Ir_{70}Ru_{30}$/CeO_2 reference sample.

Table S1. A comparison of catalytic performance of the 600 °C-annealed $Ir_{70}Ru_{30}$-B/CeO_2 and representative $N_2H_4 \cdot H_2O$ decomposition catalysts from open literatures.

Catalyst	Temperature (°C)	Reaction rate (h^{-1})	H_2 selectivity (%)	NaOH concentration (M)	E_a (kJ mol^{-1})	Ref.
$Rh_{0.8}Ni_{0.2}$/MIL-101	50	428.6	100	0.5	49.8	1
$Ni_{60}Pt_{40}$/NC	50	1602	100	2.0	48.3	2
$NiPt_{0.057}/Al_2O_3$	30	16.5	97	0	34.0	3
CoPt/$La(OH)_3$	50	2400	100	3.5	45.2	4
$Rh_{47}Ni_{18}P_{35}$@MOF-74	50	715.4	100	2	49.39	5
$Ni_{0.6}Pt_{0.4}$/g-C_3N_4	50	2194	100	0.75	35.9	6
$Pt_{0.5}Ni_{0.5}$/NGNs-850	50	2116	100	1	32.28	7
$Rh_{58}Ni_{42}$@MIL-101	50	344	100	0.5	33	8
NiFe/$CeZrO_2$	70	119.2	100	2.5	50.4	9
Ni_{10}Mo/Ni-Mo-O	50	54.5	100	2	55	10
Ni-CeO_2@SiO_2	70	219.5	100	2	59.26	11
$Ni_{0.75}Ir_{0.25}/La_2O_2CO_3$	50	330	100	1.2	65.5	12
$Ir_{70}Ru_{30}$-B/CeO_2	50	11510	86	2	41.2	This work

Table S2. Surface Ir/Ru atomic ratio of the $Ir_{70}Ru_{30}$-B/CeO_2 catalysts as determined by XPS analyses.

Sample	Ir/Ru ratio
$Ir_{70}Ru_{30}$-B/CeO_2 (as-prepared)	2.58
$Ir_{70}Ru_{30}$-B/CeO_2 (post-annealed at 600 °C)	2.60
$Ir_{70}Ru_{30}$-B/CeO_2 (post-used)	2.63

References

1. Z. Zhang, S. Zhang, Q. Yao, G. Feng, M. Zhu, Z.H. Lu, Metal-organic framework immobilized RhNi alloy nanoparticles for complete H2 evolution from hydrazine borane and hydrous hydrazine, Inorg. Chem. Front. 5(2018) 370−377.
2. Y.P. Qiu, Q. Shi, L.L. Zhou, M.H. Chen, C. Chen, P.P. Tang, G.S. Walker, P. Wang, NiPt nanoparticles anchored onto hierarchical nanoporous N-doped carbon as an efficient catalyst for hydrogen generation from hydrazine monohydrate, ACS Appl. Mater. Interfaces 12(2020) 18617−18624.
3. L. He, Y. Huang, A. Wang, Y. Liu, X. Liu, X. Chen, J.J. Delgado, X. Wang, T. Zhang, Surface modification of Ni/Al2O3 with Pt: highly efficient catalysts for H2 generation via selective decomposition of hydrous hydrazine, J. Catal. 298(2013) 1−9.
4. K. Wang, Q. Yao, S. Qing, Z.H. Lu, La(OH)3 nanosheet supported CoPt nanoparticles: a highly efficient and magnetically recyclable catalyst for hydrogen

production from hydrazine in aqueous solution, J. Mater. Chem. A 7(2019) 9903−9911.
5. R. Jiang, X. Qu, F. Zeng, Q. Li, X. Zheng, Z. Xu, J. Peng, MOF-74-immobilized ternary Rh-Ni-P nanoparticles as highly efficient hydrous hydrazine dehydrogenation catalysts in alkaline solutions, Int. J. Hydrogen Energy 44(2019) 6383−6391.
6. C. Wan, L. Sun, L. Xu, D.G. Cheng, F. Chen, X. Zhan, Y. Yang, Novel NiPt alloy nanoparticle decorated 2D layered g-C3N4 nanosheets: a highly efficient catalyst for hydrogen generation from hydrous hydrazine, J. Mater. Chem. A 7(2019) 8798−8804.
7. A. Kumar, X. Yang, Q. Xu, Ultrafine bimetallic Pt-Ni nanoparticles immobilized on 3-dimensional N-doped graphene networks: a highly efficient catalyst for dehydrogenation of hydrous hydrazine, J. Mater. Chem. A 7(2019) 112−115.
8. P. Zhao, N. Cao, W. Luo, G. Cheng, Nanoscale MIL-101 supported RhNi nanoparticles: an efficient catalyst for hydrogen generation from hydrous hydrazine, J. Mater. Chem. A 3(2015) 12468−12475.
9. H. Zou, Q. Yao, M. Huang, M. Zhu, F. Zhang, Z. H. Lu, Noble-metal-free NiFe nanoparticles immobilized on nano CeZrO2 solid solutions for highly efficient hydrogen production from hydrous hydrazine, Sustain. Energy Fuels 3(2019) 3071−3077.
10. Y.P. Qiu, G.X. Cao, H. Wen, Q. Shi, H. Dai. P. Wang, High-capacity hydrogen generation from hydrazine monohydrate using a noble-metal-free Ni10Mo/Ni-Mo-O nanocatalyst, Int. J. Hydrogen Energy 44(2019) 15110−15117.
11. M.L. Huang, Q.L. Yao, G. Feng, H.T. Zou, Z.H. Lu, Nickel-ceria nanowires embedded in microporous silica: controllable synthesis, formation mechanism, and catalytic applications, Inorg. Chem. 59(2020) 5781–5790.
12. X.L. Hong, Q.L. Yao, M.L. Huang, H.X. Du, Z.H. Lu**,** Bimetallic NiIr nanoparticles supported on lanthanum oxy-carbonate as highly efficient catalysts for hydrogen evolution from hydrazine borane and hydrazine, Inorg. Chem. Front. 6**(**2019) 2271–2278.